Uncertainty and Disturbance Estimator-Based Robust Trajectory Tracking Control for a Quadrotor in a Global Positioning System-Denied Environment

Qi Lu
Department of Mechanical Engineering,
Texas Tech University,
Lubbock, TX 79409
e-mail: qi.lu@ttu.edu

Beibei Ren[1]
Department of Mechanical Engineering,
Texas Tech University,
Lubbock, TX 79409
e-mail: beibei.ren@ttu.edu

Siva Parameswaran
Department of Mechanical Engineering,
Texas Tech University,
Lubbock, TX 79409
e-mail: siva.parameswaran@ttu.edu

Qing-Chang Zhong
Department of Electrical and
Computer Engineering,
Illinois Institute of Technology,
Chicago, IL 60616
e-mail: zhongqc@ieee.org

This paper addresses the problem of autonomous trajectory tracking control for a quadrotor in a global positioning system (GPS)-denied environment using only onboard sensing. To achieve that goal, it requires accurate estimation of quadrotor states followed by proper control actions. For the position estimation in a GPS-denied environment, an open source high speed optical flow sensor PX4FLOW is adopted. As for the quadrotor control, there are several challenges due to its highly nonlinear system dynamics, such as underactuation, coupling, model uncertainties, and external disturbances. To deal with those challenges, the cascaded inner–outer uncertainty and disturbance estimator (UDE)-based robust control scheme has been developed and applied to the attitude and position control of a quadrotor. Extensive real flight experiments, including attitude stabilization, hover, disturbance rejection, trajectory tracking, and comparison with the proportional–integral–derivative (PID) controller are carried out to demonstrate the effectiveness of the developed UDE-based controllers. [DOI: 10.1115/1.4037736]

Keywords: uncertainty and disturbance estimator (UDE), quadrotor, position control, attitude control, robust control, GPS-denied navigation

1 Introduction

In past years, unmanned aerial vehicles (UAVs) have drawn considerable amount of attention from both research and industrial communities because of its wide field of applications, such as search and rescue, industrial inspection, precision agriculture, aerial photography, and so forth [1–5]. For those applications, the abilities of the UAVs to navigate autonomously, maneuver sharply, and hover precisely are very important. Among all kinds of UAVs, the quadrotor has the attracting features of low cost, easy deployment, and vertical takeoff and landing. It is widely used by the researchers as the validation platform. The challenges that lie in the autonomy of the quadrotor are two-folded. The first aspect is the accurate state estimation of the vehicle. Another aspect is the motion control algorithm development for such highly nonlinear system [6,7].

A quadrotor has six degrees-of-freedom including rotational (attitude) and translational (position) motions. The attitude angles are easy to estimate using onboard inertia measurement unit (IMU). However, without position feedback control, the quadrotor is likely to drift over time due to the inaccurate measurement of the low-cost onboard IMU or other environmental disturbance, such as wind. The global positioning system (GPS) receiver is a common onboard device utilized for the navigation task of the quadrotor UAVs [4,8,9]. It relies on the satellites to determine the quadrotor positions, thus requiring a clear view of the sky. Such constraint has limited the GPS mostly for outdoor applications. As for the motion estimation of UAVs in GPS-denied environments, the existing methods could be roughly divided into two categories, offboard methods and onboard methods. One of the widely adopted offboard methods is the motion capture system, which utilizes multiple external cameras and reflective markers to determine the position of a quadrotor. It has the advantages of submillimeter accuracy and fast update rate [10–12]. However, it is not suitable for missions where the installation of such a system is not feasible. Therefore, for UAVs, how to extract their position information in GPS-denied environments solely from the onboard sensing is still a very challenging and open research topic [6].

The laser range finder is one of the commonly used onboard sensors for GPS-denied navigation tasks [13–17]. The position of the quadrotor is estimated by fusing the laser range finder data with the IMU data in a simultaneous localization and mapping framework, which also accomplishes the map building task. The advantages of laser-based localization method lie in that it works in dark, featureless environment, such as tunnels [13,17]. However, the laser range finder may exceed the payload limit of small size UAVs [18] while the camera having the advantage of lightweight and low cost. Considering the payload and energy constraints, the vision-based onboard sensing system could be an effective solution to provide the vehicle position state estimations. Recent studies have revealed that flying insects utilize optical flow to accomplish their dynamic navigation while keeping energy consumption at an unbelievable low level [19]. This biomimetic principle motivates a number of researchers exploring the idea of optical flow-based navigation [20,21]. Compared to other vision-based algorithms, such as artificial marker detection [6,22], the optical flow-based approach works without the aid of markers. Moreover, it is relatively computationally efficient compared with visual-based simultaneous localization and mapping [18]. The limitation of the optical flow-based approach lies in the requirement for the working environment. As a visual-based

[1]Corresponding author.

Contributed by the Dynamic Systems Division of ASME for publication in the Journal of Dynamic Systems, Measurement, and Control. Manuscript received March 21, 2016; final manuscript received August 16, 2017; published online November 8, 2017. Assoc. Editor: Manish Kumar.

localization method, it needs adequate lighting and textured environment to provide the reliable estimation. The advantages and limitations of the major existing onboard position estimation methods are summarized in Table 1. In Ref. [7], an open source high speed optical flow sensor PX4FLOW is developed, which utilizes the camera and sonar to estimate the horizontal velocity and altitude information of a quadrotor. In this paper, the PX4FLOW optical flow sensor is adopted to accomplish the quadrotor position estimation task in a GPS-denied environment which is motivated by two aspects of considerations. First, the experimental platform, Hummingbird quadrotor from Ascending Technologies GmbH (AscTec) [23], has limited payload capacity, which is about 200 g. Compared with laser, the PX4FLOW sensor only weights about 20 g. Second, the PX4FLOW optical flow sensor estimates the optical flow at a high update rate with angular rate compensation and distance scaling. Such features make it especially suitable for quadrotor navigation task.

Besides the difficulties of motion estimation in GPS-denied environments, the challenges for the autonomous control of UAVs also come from its highly nonlinear dynamics. First of all, the quadrotor is an open-loop unstable system. Due to its fast dynamics, it requires fast controller update rate to maintain the stability of the system. Hence, controllers with low computational complexities are desired. Second, the quadrotor is an underactuated multiple-input multiple-output system, which has six outputs while only four inputs. The horizontal positions (x, y) of a quadrotor are controlled by varying its attitude angles. Third, the model uncertainties which are caused by aerodynamic effects, battery voltage dropping, and payload change, make it very difficult to obtain the accurate physical model and related parameters. Fourth, strongly coupled dynamics and nonaffine inputs for horizontal motion subsystems also bring difficulties for controller design. Finally, the quadrotor is very sensitive to external disturbance generated by complex working environment due to its small size and lightweight.

In order to deal with those challenges and to achieve the good control performance, many control strategies have been reported in literature. The effectiveness of the classical proportional–integral–derivative (PID) controllers and linear-quadratic regulator was investigated in Refs. [24,25]. However, those methods are developed based on the linearized quadrotor dynamics [8,26]. To confront the nonlinearities existing in quadrotor dynamics, various nonlinear control techniques have been developed. A two-loop structure with a dynamic inversion inner loop and a robust internal dynamics stabilization outer loop has been proposed in Ref. [27] to deal with the problem of underactuation and system coupling. The accurate model knowledge is a necessary condition for the good performance of dynamic inversion. However, in practice, the quadrotor may deviate from the nominal model due to the model uncertainty and perturbation of external disturbance. Backstepping is a well-known technique used for control of nonlinear systems, and it is well suited for the cascaded structure of the quadrotor dynamics to solve the underactuation problem [28,29]. However, the classical backstepping technique requires full knowledge of the plant and states, making it prone to instability for model uncertainty [29].

Regarding the compensation of model uncertainties, adaptive control methods are widely used, such as the model reference adaptive control [30], the immersion and invariance-based adaptive control [26], and adaptation laws based on Lyapunov-like energy function [12]. The robustness is crucial to the UAVs, since they are constantly perturbed by external disturbances, especially in outdoor applications. Hence, robust control of a quadrotor is still an active field. Without considering the presence of disturbances, the stability and tracking performance may be degraded [12]. In Ref. [31], a controller based on sliding mode disturbance observer is applied to quadrotor attitude and position control in the presence of external disturbances. A robust nonlinear attitude control method is proposed in Ref. [32] where the external disturbances are compensated by the designed robust compensator. The effectiveness of the disturbance observer-based control method for attitude and position control is investigated in Refs. [33,34].

Compared to the aforementioned robust control methods, the uncertainty and disturbance estimator (UDE)-based controller, which was proposed in Ref. [35], has relatively simple structure and is computationally efficient. The basic idea of the UDE method is that in the frequency domain, an engineering signal (the model uncertainty and external disturbance) can be approximated by putting it through a filter with the appropriate bandwidth. The remarkable performance of the UDE strategy has been demonstrated in recent years through both theories (including extensions to both linear [35,36] and nonlinear systems [37–40], systems with delays [36,40], etc.) and practical applications (covering mechatronics and robotics [41–44], electrical machines, and drives [35,39]).

In this paper, in response to the aforementioned challenges, the PX4FLOW smart camera is first integrated to accomplish the navigation task in a GPS-denied environment. Second, a robust tracking control scheme for a quadrotor based on the UDE is developed to achieve the full degrees-of-freedom control of a quadrotor. The underactuation problem is solved by utilizing the cascaded inner-outer loop control structure. Then, the UDE-based attitude and position controllers are derived to deal with system coupling, nonaffine input, internal model uncertainty, and external disturbance. Finally, the effectiveness of the developed control strategy is demonstrated through real flight experimental studies. The main contributions of this paper are as follows:

(1) The UDE-based inner–outer cascaded control scheme for a quadrotor is developed and applied to quadrotor position control to achieve the trajectory tracking in a GPS-denied environment using only onboard sensors. In particular, the

Table 1 Comparison of position estimation methods

Methods	Advantages	Limitations
Laser	Works in dark environment [13] Works in featureless environment [13] Map building simultaneously [14]	Heavy [18] Costly Computationally expensive
Artificial marker	Drift-free position information [6] Orientation information [22]	Artificial marker setup Adequate lighting
Visual-based simultaneous localization and mapping	Drift-free position information [18] Map building simultaneously	Textured environment Adequate lighting Computationally expensive
PX4FLOW	Light weight Low cost Computationally efficient [19] Fast update rate [7]	Textured environment Adequate lighting

PX4FLOW smart camera is integrated to accurately estimate the quadrotor position and velocity information.

(2) Motivated by Ren et al. [39], the UDE-based method is applied to deal with the nonaffine inputs for the horizontal position (x, y) control. The developed method avoids the singularity problem which could be caused by the construction of the inverse trigonometric function operator.

(3) The UDE-based method is applied to quadrotor attitude control to deal with coupling effects, model uncertainties, and external disturbances.

(4) Compared with previous UDE works on quadrotor attitude and altitude control [43,44], this paper extends the UDE method to the full degrees-of-freedom control of a quadrotor. Additionally, the performance of the attitude control is further improved.

The rest of the paper is organized as follows: Section 2 illustrates the system modeling about the quadrotor dynamics and formulates the problem. Section 3 presents the details of UDE-based controller development. Section 4 shows the proof of closed-loop system stability and the performance analysis. The effectiveness of the proposed approach is demonstrated through extensive real flight experiments in Sec. 5. Conclusions are made in Sec. 6.

2 System Modeling and Problem Formulation

As shown in Fig. 1, the quadrotor is a helicopter consisting of four rotors on each corner with two of them (1 and 3) rotating clockwise and the other two (2 and 4) rotating counterclockwise. The motion of the quadrotor is controlled by varying the speeds of four rotors.

The mathematical model used in this paper is under these assumptions. The structure of the quadrotor is rigid and symmetric; thus, the geometric center and the center of gravity of quadrotor are coincident with each other. The thrust and torque generated by each rotor are proportional to the square of the rotor speed. Let $\mathcal{I} = \{x_I \quad y_I \quad z_I\}$ denotes a right-hand inertial frame with z_I being the vertical direction axis pointing toward the ground. The body fixed frame $\mathcal{B} = \{x_B \quad y_B \quad z_B\}$ is rigidly attached to the center of gravity of quadrotor. The thrust f_k and torque τ_k generated by each rotor could be described as

$$\begin{aligned} f_k &= h_F \omega_k^2 \\ \tau_k &= h_M \omega_k^2, \quad k = 1 \ldots 4 \end{aligned} \tag{1}$$

where ω_k is kth motor speed, h_F is a positive thrust constant, and h_M is a positive drag constant. The total lift force F and torques τ_ϕ, τ_θ, and τ_ψ along the quadrotor body axes can be expressed as

$$\begin{aligned} F &= f_1 + f_2 + f_3 + f_4 \\ &= h_F(\omega_1^2 + \omega_2^2 + \omega_3^2 + \omega_4^2) \\ \tau_\phi &= l(f_4 - f_2) = h_F l(\omega_4^2 - \omega_2^2) \\ \tau_\theta &= l(f_1 - f_3) = h_F l(\omega_1^2 - \omega_3^2) \\ \tau_\psi &= \tau_2 + \tau_4 - \tau_1 - \tau_3 \\ &= h_M(\omega_2^2 + \omega_4^2 - \omega_1^2 - \omega_3^2) \end{aligned} \tag{2}$$

where l denotes the quadrotor arm length, which is the distance between the z_B axis and the motor axis. The Euclidean position and the Euler angle of the quadrotor with respect to the inertial frame are represented by $\xi = [x \quad y \quad z]^{\mathrm{T}}$ and $\eta = [\phi \quad \theta \quad \psi]^{\mathrm{T}}$. Assume that there exist bounded disturbance signals $d_{\eta i}$, $i = 1 \ldots 3$ for attitude subsystems and $d_{\xi j}$, $j = 1 \ldots 3$ for position subsystems, which may be caused by wind gusts or other environmental factors. By applying small angle approximation, the dynamics of the quadrotor in the inertial frame could be described using the following six equations [2]:

$$\ddot{\phi} = \frac{1}{I_x}\left[\tau_\phi + (I_y - I_z)\dot{\theta}\dot{\psi} - J\dot{\theta}\Omega\right] + d_{\eta 1} \tag{3}$$

$$\ddot{\theta} = \frac{1}{I_y}\left[\tau_\theta + (I_z - I_x)\dot{\phi}\dot{\psi} + J\dot{\phi}\Omega\right] + d_{\eta 2} \tag{4}$$

$$\ddot{\psi} = \frac{1}{I_z}\left[\tau_\psi + (I_x - I_y)\dot{\theta}\dot{\phi}\right] + d_{\eta 3} \tag{5}$$

$$\ddot{x} = -\frac{F}{m}\left[\cos(\psi)\sin(\theta)\cos(\phi) + \sin(\psi)\sin(\phi)\right] + d_{\xi 1} \tag{6}$$

$$\ddot{y} = -\frac{F}{m}\left[\sin(\psi)\sin(\theta)\cos(\phi) - \cos(\psi)\sin(\phi)\right] + d_{\xi 2} \tag{7}$$

$$\ddot{z} = -\frac{F}{m}\left[\cos(\theta)\cos(\phi)\right] + g + d_{\xi 3} \tag{8}$$

where I_x, I_y, and I_z are the quadrotor moments of inertia along the x_B, y_B, and z_B axes, g is the gravitational acceleration represented in the inertia frame, m is the mass, J denotes the inertia of the propeller, and $\Omega = \omega_2 + \omega_4 - \omega_1 - \omega_3$.

The desired reference trajectory is given as $[x_r \quad y_r \quad z_r \quad \psi_r]^{\mathrm{T}}$, which is continuous differentiable and bounded up to its second-order time derivative. The overall control objective is to develop the UDE-based robust control algorithms for the quadrotor system

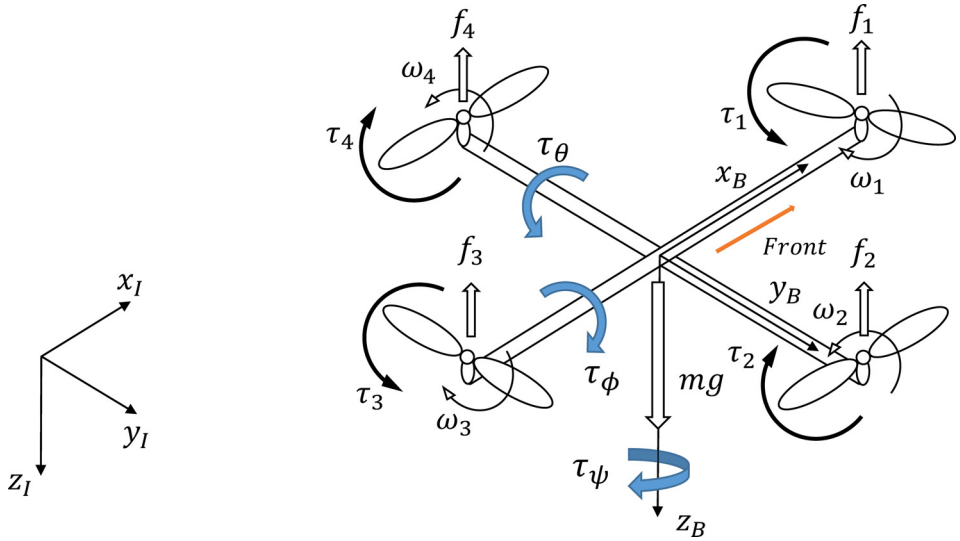

Fig. 1 Coordinate systems for a quadrotor model

to drive the states $[x \quad y \quad z \quad \psi]^T$ to asymptotically track the reference signals $[x_r \quad y_r \quad z_r \quad \psi_r]^T$.

3 Control System Design

In this section, the UDE-based attitude and position controllers will be developed following the procedures in Refs. [35,39]. The block diagram of the overall control system is shown in Fig. 2. The underactuation is solved by introducing the cascaded inner–outer loop control structure. Furthermore, the filtered tracking error is utilized to simplify the controller development and implementation.

3.1 Attitude Controller. The UDE-based controllers for quadrotor attitude stabilization and tracking are designed in this subsection. Choosing the generalized coordinates as $\eta_1 = \phi$, $\eta_2 = \theta$, and $\eta_3 = \psi$, the reference signals as $\eta_{r1} = \phi_r$, $\eta_{r2} = \theta_r$, and $\eta_{r3} = \psi_r$, which are continuous differentiable and bounded up to its second-order time derivative, the filtered tracking errors as $\varepsilon_{\eta 1} = \varepsilon_\phi$, $\varepsilon_{\eta 2} = \varepsilon_\theta$, $\varepsilon_{\eta 3} = \varepsilon_\psi$ and the control inputs as $u_{\eta 1} = \tau_\phi$, $u_{\eta 2} = \tau_\theta$, $u_{\eta 3} = \tau_\psi$, the attitude dynamics (3)–(5) could be written as

$$\ddot{\eta}_i = D_{\eta i} + B_{\eta i} u_{\eta i} \tag{9}$$

where $i = 1 \ldots 3$ denote the roll, pitch, yaw, respectively, $B_{\eta 1} = 1/I_x$, $B_{\eta 2} = 1/I_y$, $B_{\eta 3} = 1/I_z$, and

$$\begin{aligned} D_{\eta 1} &= \frac{1}{I_x}\left[(I_y - I_z)\dot{\theta}\dot{\psi} - J\dot{\theta}\Omega\right] + d_{\eta 1} \\ D_{\eta 2} &= \frac{1}{I_y}\left[(I_z - I_x)\dot{\phi}\dot{\psi} + J\dot{\phi}\Omega\right] + d_{\eta 2} \\ D_{\eta 3} &= \frac{1}{I_z}\left[(I_x - I_y)\dot{\theta}\dot{\phi}\right] + d_{\eta 3} \end{aligned} \tag{10}$$

are the lumped uncertainty terms, which include the coupling terms $[(I_y - I_z)/I_x]\dot{\theta}\dot{\psi}$, $[(I_z - I_x)/I_y]\dot{\phi}\dot{\psi}$ and $[(I_x - I_y)/I_z]\dot{\theta}\dot{\phi}$ generated by gyroscopic effects, uncertainty terms $-J\dot{\theta}\Omega/I_x$ and $J\dot{\phi}\Omega/I_y$ since the rotor inertia J is an unknown positive constant, and the bounded disturbance terms $d_{\eta 1}$, $d_{\eta 2}$, and $d_{\eta 3}$. From Eq. (9), it is worth noting that the attitude subsystems have been decoupled into three separated subsystems.

The attitude and angular velocity tracking errors are defined as

$$\begin{aligned} e_{\eta i} &= \eta_{ri} - \eta_i \\ \dot{e}_{\eta i} &= \dot{\eta}_{ri} - \dot{\eta}_i \end{aligned} \tag{11}$$

and the filtered tracking errors are defined as

$$\varepsilon_{\eta i} = \lambda_{\eta i} e_{\eta i} + \dot{e}_{\eta i} \tag{12}$$

where $\lambda_{\eta i}$ are positive design parameters. The time derivative of the filtered tracking error (12) is given by

$$\dot{\varepsilon}_{\eta i} = \lambda_{\eta i}\dot{e}_{\eta i} + \ddot{\eta}_{ri} - D_{\eta i} - B_{\eta i} u_{\eta i} \tag{13}$$

If all states are measurable, then the controller could be designed as

$$B_{\eta i} u_{\eta i} = \lambda_{\eta i}\dot{e}_{\eta i} + \ddot{\eta}_{ri} + u^d_{\eta i} + k_{\eta i}\varepsilon_{\eta i} \tag{14}$$

using feedback linearization, with the desired error dynamics

$$\dot{\varepsilon}_{\eta i} = -k_{\eta i}\varepsilon_{\eta i} \tag{15}$$

where $k_{\eta i}$ are positive control gains, and $u^d_{\eta i} = -D_{\eta i}$ are the lumped uncertainty compensation terms. The desired error dynamics (15) shows that the filtered tracking errors will exponentially converge to zero as time goes to infinity. The convergence rate could be adjusted by tuning the control gains $k_{\eta i}$. Nevertheless, the lumped uncertainty terms $D_{\eta i}$ in Eq. (13) could not be directly measured due to the system uncertainty and disturbance; thus, $u^d_{\eta i}$ in Eq. (14) should be redesigned. Substituting Eq. (14) into Eq. (13) leads to

$$\dot{\varepsilon}_{\eta i} = -k_{\eta i}\varepsilon_{\eta i} - D_{\eta i} - u^d_{\eta i} \tag{16}$$

solving for the lumped uncertainty terms results in

$$D_{\eta i} = -\dot{\varepsilon}_{\eta i} - k_{\eta i}\varepsilon_{\eta i} - u^d_{\eta i} \tag{17}$$

It indicates that the lumped uncertainty terms could be observed by the filtered tracking errors and the control input signals. However, it could not be directly applied in the control law. Following the techniques provided in Ref. [35], adopting strictly proper low-pass filters $G^f_{\eta i}(s)$ with unity gain and zero phase shift over the spectrum of $D_{\eta i}$, then the lumped uncertainty terms $D_{\eta i}$ could be accurately approximated as

$$\hat{D}_{\eta i} = \mathcal{L}^{-1}[G^f_{\eta i}(s)] * [-\dot{\varepsilon}_{\eta i} - k_{\eta i}\varepsilon_{\eta i} - u^d_{\eta i}] \tag{18}$$

where $\mathcal{L}^{-1}(\cdot)$ is the inverse-Laplace transform operator and "*" is the convolution operator. Substituting $u^d_{\eta i} = -\hat{D}_{\eta i}$ into Eq. (18) leads to

$$u^d_{\eta i} = \mathcal{L}^{-1}[G^f_{\eta i}(s)] * [\dot{\varepsilon}_{\eta i} + k_{\eta i}\varepsilon_{\eta i} + u^d_{\eta i}] \tag{19}$$

solving for $u^d_{\eta i}$ results in

$$u^d_{\eta i} = \mathcal{L}^{-1}\left[\frac{G^f_{\eta i}(s)}{1 - G^f_{\eta i}(s)}\right] * [\dot{\varepsilon}_{\eta i} + k_{\eta i}\varepsilon_{\eta i}] \tag{20}$$

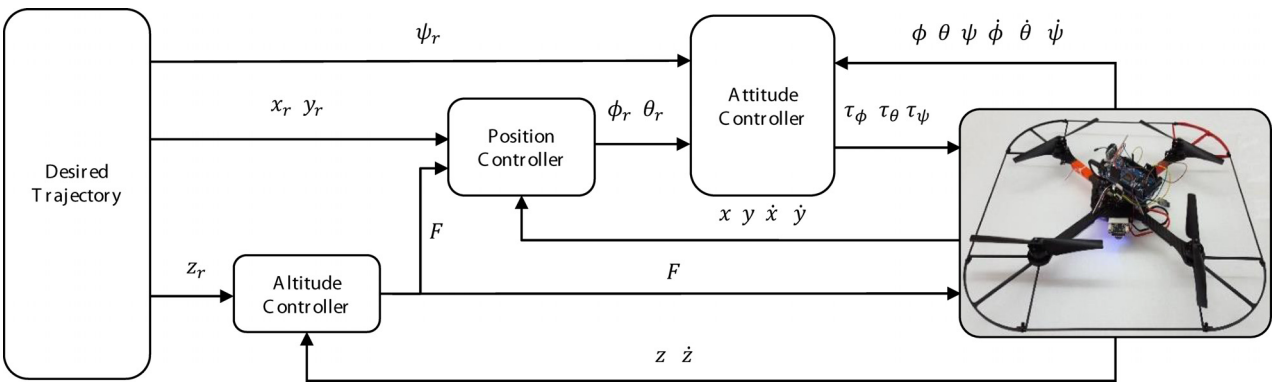

Fig. 2 Quadrotor control scheme

Combining Eqs. (14) and (20) leads to the attitude controllers

$$u_{\eta i}=\frac{1}{B_{\eta i}}\left\{k_{\eta i}\varepsilon_{\eta i}+\lambda_{\eta i}\dot{e}_{\eta i}+\ddot{\eta}_{ri}+\mathcal{L}^{-1}\left[\frac{G^f_{\eta i}(s)}{1-G^f_{\eta i}(s)}\right]*\left[\dot{\varepsilon}_{\eta i}+k_{\eta i}\varepsilon_{\eta i}\right]\right\} \tag{21}$$

where $i=1\ldots3$ denote the roll, pitch, and yaw, respectively.

3.2 Position Controller. From the cascaded control structure of the quadrotor (Fig. 2), it could be seen that the horizontal motions of the quadrotor are controlled through varying its attitude angles. However, the control inputs for horizontal motions are expressed in nonaffine forms, which lead to the failure of using feedback linearization. The constructions of inverse trigonometric operators may lead to singularity problems, since the domain of the $\sin^{-1}(*)$ function is $-1\le *\le 1$. In order to deal with this problem, techniques in Ref. [39] are adopted such that $\sin(\theta_r)$ and $\sin(\phi_r)$ are approximated using $K_x\theta_r$ and $K_y\phi_r$. The approximation errors, coupling terms, and disturbances are treated as the lumped uncertainty terms.

Since only onboard sensors are used to measure the positions of the quadrotor, it is assumed that the quadrotor body frame is initially aligned with the inertial frame and the heading of the quadrotor is always pointing to the positive x_I axis. Then, it is reasonable to design the virtual control inputs for the horizontal motion as

$$u_x=K_x\theta_r\cos(\phi) \tag{22}$$

$$u_y=-K_y\phi_r \tag{23}$$

By choosing the generalized coordinates as $\xi_1=x$, $\xi_2=y$, $\xi_3=z$, the reference signals as $\xi_{r1}=x_r$, $\xi_{r2}=y_r$, $\xi_{r3}=z_r$, which are continuous differentiable and bounded up to its second-order time derivative, the filtered tracking errors as $\varepsilon_{\xi1}=\varepsilon_x$, $\varepsilon_{\xi2}=\varepsilon_y$, $\varepsilon_{\xi3}=\varepsilon_z$, the position dynamics (6), (7), and (8) can be written as

$$\ddot{\xi}_j=-B_{\xi j}u_{\xi j}+\bar{g}_j+D_{\xi j} \tag{24}$$

where $j=1\ldots3$ denote the x, y, and z, respectively, $B_{\xi1}=B_{\xi2}=F/m, B_{\xi3}=1/m, \bar{g}_1=\bar{g}_2=0, \bar{g}_3=g, u_{\xi1}=u_x, u_{\xi2}=u_y, u_{\xi3}=F$, and

$$\begin{aligned}
D_{\xi1}&=-\frac{F}{m}\left[\cos(\psi)\sin(\theta)\cos(\phi)+\sin(\psi)\sin(\phi)-u_x\right]+d_{\xi1}\\
D_{\xi2}&=-\frac{F}{m}\left[\sin(\psi)\sin(\theta)\cos(\phi)-\cos(\psi)\sin(\phi)-u_y\right]+d_{\xi2}\\
D_{\xi3}&=\frac{F}{m}\left[1-\cos(\theta)\cos(\phi)\right]+d_{\xi3}
\end{aligned} \tag{25}$$

are the lumped uncertainty terms. It should be noted that there are two benefits of this technique. First, the controller is designed based on the nonlinear dynamics of the horizontal motion without linearization. The effects of the approximation error, coupling terms, and disturbances will be estimated and compensated by the UDE. Second, the control inputs are in affine forms, which avoid the singularity problems that may be brought by the constructions of inverse operators. The position and velocity tracking errors are defined as

$$\begin{aligned}
e_{\xi j}&=\xi_{rj}-\xi_j\\
\dot{e}_{\xi j}&=\dot{\xi}_{rj}-\dot{\xi}_j
\end{aligned} \tag{26}$$

and the filtered tracking errors are defined as

$$\varepsilon_{\xi j}=\lambda_{\xi j}e_{\xi j}+\dot{e}_{\xi j} \tag{27}$$

where $\lambda_{\xi j}$ are positive design parameters.

Similar controller design procedures that are described in Sec. 3.1 are followed to derive the UDE-based position controllers

$$u_{\xi j}=\frac{1}{B_{\xi j}}\bar{g}_j-\frac{1}{B_{\xi j}}\left\{k_{\xi j}\varepsilon_{\xi j}+\lambda_{\xi j}\dot{e}_{\xi j}+\ddot{\xi}_{rj}+\mathcal{L}^{-1}\left[\frac{G^f_{\xi j}(s)}{1-G^f_{\xi j}(s)}\right]*\left[\dot{\varepsilon}_{\xi j}+k_{\xi j}\varepsilon_{\xi j}\right]\right\} \tag{28}$$

where $j=1\ldots3$ denote the x, y, and z, respectively, $k_{\xi j}$ are positive control gains, and $G^f_{\xi j}(s)$ are low pass filters which cover the spectrum of lumped uncertainty terms $D_{\xi j}$.

4 Stability and Performance Analysis

4.1 Stability Analysis. Define the system tracking errors as $e_1=e_{\eta1}$, $e_2=e_{\eta2}$, $e_3=e_{\eta3}$, $e_4=e_{\xi1}$, $e_5=e_{\xi2}$, $e_6=e_{\xi3}$, the filtered tracking errors as $\varepsilon_1=\varepsilon_{\eta1}$, $\varepsilon_2=\varepsilon_{\eta2}$, $\varepsilon_3=\varepsilon_{\eta3}$, $\varepsilon_4=\varepsilon_{\xi1}$, $\varepsilon_5=\varepsilon_{\xi2}$, $\varepsilon_6=\varepsilon_{\xi3}$, the related controller parameters as $\lambda_1=\lambda_{\eta1}$, $\lambda_2=\lambda_{\eta2}$, $\lambda_3=\lambda_{\eta3}$, $\lambda_4=\lambda_{\xi1}$, $\lambda_5=\lambda_{\xi2}$, $\lambda_6=\lambda_{\xi3}$, and the estimation errors of the lumped uncertainty terms as

$$\tilde{D}_i\triangleq D_i-\hat{D}_i \tag{29}$$

where $D_1=D_{\eta1}, D_2=D_{\eta2}, D_3=D_{\eta3}, D_4=D_{\xi1}, D_5=D_{\xi2}, D_6=D_{\xi3}$, $\hat{D}_i$ are the estimations of D_i. Substituting Eq. (21) into Eq. (9) and Eq. (28) into Eq. (24) results in the following closed-loop filtered tracking error dynamics:

$$\dot{\varepsilon}_i=-k_i\varepsilon_i-\tilde{D}_i \tag{30}$$

where $i=1\ldots6$ denote the ϕ, θ, ψ, x, y, and z, respectively, and $k_1=k_{\eta1}$, $k_2=k_{\eta2}$, $k_3=k_{\eta3}$, $k_4=k_{\xi1}$, $k_5=k_{\xi2}$, $k_6=k_{\xi3}$. Since the low-pass filters $G^f_1(s)=G^f_{\eta1}(s), G^f_2(s)=G^f_{\eta2}(s), G^f_3(s)=G^f_{\eta3}(s)$, $G^f_4(s)=G^f_{\xi1}(s), G^f_5(s)=G^f_{\xi2}(s), G^f_6(s)=G^f_{\xi3}(s)$ are adopted to estimate the lumped uncertainty terms, the estimation errors are rewritten as

$$\tilde{D}_i=\mathcal{L}^{-1}[1-G^f_i(s)]*D_i \tag{31}$$

THEOREM 1. *Consider the closed-loop system dynamics that is characterized by the quadrotor plant (9), (24), and the UDE-based control laws (21), (28). Given the initial tracking errors $e_i(0)$ and the initial filtered tracking errors $\varepsilon_i(0)$, the tracking errors $e_i(t)$ are bounded by a compact set $\Omega_{e_i}:=\{e_i(t)\in\mathbb{R}||e_i(t)|\le max\{e_i(0),\gamma_{\varepsilon_i},\gamma_i\}\}$ for all $t\ge0$, where $\gamma_{\varepsilon i}=[k_i\varepsilon_i(0)-\bar{D}_i]/[k_i(\lambda_i-k_i)]$ and $\gamma_i=\bar{D}_i/(k_i\lambda_i)$. The size of the compact set Ω_{e_i} can be adjusted by the controller parameters λ_i, k_i, the initial conditions $e_i(0)$, $\varepsilon_i(0)$, and the upper bounds of the lumped uncertainty term estimation errors $\bar{\tilde{D}}_i$.*

Proof. Solving Eq. (30), Eqs. (12) and (27) for ε_i and e_i results in

$$\varepsilon_i(t)=\varepsilon_i(0)\exp(-k_it)-\exp(-k_it)\int_0^t\tilde{D}_i(\zeta)\exp(k_i\zeta)d\zeta \tag{32}$$

$$e_i(t)=e_i(0)\exp(-\lambda_it)+\exp(-\lambda_it)\int_0^t\varepsilon_i(\zeta)\exp(\lambda_i\zeta)d\zeta \tag{33}$$

where $\exp(*)$ represents the exponential function. It is easy to conclude that the lumped uncertainty terms (25) for the position subsystems are bounded due to the trigonometric functions, the physical limit of the motor speed and the bounded disturbance terms $d_{\xi i}$. Similar conclusions could be drawn for the lumped uncertainty terms of the attitude subsystems (10). Thus, it could

be concluded that the disturbance terms D_i are bounded which satisfies the following equation:

$$|D_i(t)| \leq \bar{D}_i \tag{34}$$

where $\bar{D}_i$ denote the upper bounds of the lumped uncertainty terms. Furthermore, since the filters $G_i^f(s)$ are designed to be stable filters, from Eq. (31), the lumped uncertainty estimation errors $\tilde{D}_i$ are also bounded

$$|\tilde{D}_i(t)| \leq \bar{\tilde{D}}_i \tag{35}$$

where $\bar{\tilde{D}}_i$ denote the upper bounds of the estimation errors. Combining Eqs. (35) and (32) leads to

$$\varepsilon_i(t) \leq \varepsilon_i(0)\exp(-k_i t) + \frac{\bar{\tilde{D}}_i}{k_i}[1 - \exp(-k_i t)] \tag{36}$$

Substituting Eq. (36) into Eq. (33) leads to

$$\begin{aligned} e_i(t) \leq\ & e_i(0)\exp(-\lambda_i t) + \frac{\varepsilon_i(0)}{\lambda_i - k_i}\left[\exp(-k_i t) - \exp(-\lambda_i t)\right] \\ & + \frac{\bar{\tilde{D}}_i}{k_i\lambda_i}[1 - \exp(-\lambda_i t)] - \frac{\bar{\tilde{D}}_i}{k_i(\lambda_i - k_i)}\left[\exp(-k_i t) - \exp(-\lambda_i t)\right] \\ =\ & e_i(0)\exp(-\lambda_i t) + \frac{\bar{\tilde{D}}_i}{k_i\lambda_i}[1 - \exp(-\lambda_i t)] + \frac{k_i\varepsilon_i(0) - \bar{\tilde{D}}_i}{k_i(\lambda_i - k_i)} \\ & \times \left[\exp(-k_i t) - \exp(-\lambda_i t)\right] \end{aligned} \tag{37}$$

From Eq. (37), it could be concluded that the tracking errors $e_i(t)$ are bounded for all $t \geq 0$. In other words,

$$|e_i(t)| \leq \max\{e_i(0),\ \gamma_{\varepsilon_i},\ \gamma_i\} \tag{38}$$

where $\gamma_{\varepsilon i} = [k_i\varepsilon_i(0) - \bar{\tilde{D}}_i]/[k_i(\lambda_i - k_i)]$ and $\gamma_i = \bar{\tilde{D}}_i/(k_i\lambda_i)$. As $t \to \infty$, the tracking errors $e_i(t)$ are bounded by γ_i. Hence

$$|e_i(\infty)| \leq \frac{\bar{\tilde{D}}_i}{k_i\lambda_i} \tag{39}$$

□

Remark 1. From Theorem 1, it implies that the upper bounds $\max\{e_i(0),\ \gamma_{\varepsilon_i},\ \gamma_i\}$ of the tracking errors e_i are solely affected by the initial conditions $e_i(0)$, $\varepsilon_i(0)$, the controller parameters λ_i, k_i, and the upper bounds of estimation errors $\bar{\tilde{D}}_i$ rather than the upper bounds of the lumped uncertainty terms $\bar{D}_i$. Furthermore, as t $\to \infty$, the tracking errors $e_i(t)$ are bounded by γ_i. By appropriately designing the filters $G_i^f(s)$, the upper bounds of the estimation errors could be reduced or even asymptotically converge to zero to ensure the performance and robustness of the closed-loop system.

4.2 Performance Analysis

THEOREM 2. *The closed-loop system dynamics considered above achieves asymptotic disturbance rejection performance if: (i) the closed-loop system is stable, (ii) λ_i and k_i are positive, and (iii) the filters $G_i^f(s)$ are designed appropriately as strictly proper stable filters with unity gain and zero phase shift over the spectrum of the lumped uncertainty terms D_i and zero gain elsewhere.*

Proof. Substituting Eq. (31) into Eq. (30) and taking the Laplace transform result in

$$s\Sigma_i(s) = -k_i\Sigma_i(s) - [1 - G_i^f(s)]D_i(s) \tag{40}$$

where $\Sigma_i(s)$ and $D_i(s)$ are the Laplace transform of $\varepsilon_i(t)$ and $D_i(t)$. The Laplace transform of the filtered tracking errors (12) and (27) could be written as

$$\Sigma_i(s) = \lambda_i E_i(s) + sE_i(s) \tag{41}$$

where $E_i(s)$ are the Laplace transform of the tracking errors $e_i(t)$. Substituting Eq. (41) into Eq. (40) leads to

$$E_i(s) = \frac{\left[G_i^f(s) - 1\right]}{s^2 + (\lambda_i + k_i)s + \lambda_i k_i}D_i(s) \tag{42}$$

From Eq. (34), it could be concluded that the lumped uncertainty terms D_i are bounded which satisfy the following inequality:

$$\lim_{s\to 0} sD_i(s) < \infty \tag{43}$$

If the filters $G_i^f(s)$ are designed as the strictly proper stable filters that have unity gain and zero phase shift over the spectrum of the lumped uncertainty terms D_i and zero gain elsewhere and the controller parameters λ_i and k_i are positive, by applying the final value theorem to Eq. (42), there is

$$\begin{aligned} \lim_{t\to\infty} E_i(t) &= \lim_{s\to 0} sE_i(s) \\ &= \lim_{s\to 0} \frac{s\left[G_i^f(s) - 1\right]}{s^2 + (\lambda_i + k_i)s + \lambda_i k_i}D_i(s) \\ &= 0 \end{aligned} \tag{44}$$

□

5 Experimental Validation

5.1 Experimental Testbed and Environment

5.1.1 Experimental Testbed. To verify the effectiveness and performance of the developed UDE-based controller, real flight experiments are carried out with a modified Hummingbird quadrotor from AscTec [23], which is shown in Fig. 3. The mass of this quadrotor including sensors and payloads is 675 g. The onboard IMU could provide the angle ϕ, θ, ψ and the angular velocity $\dot{\phi}$, $\dot{\theta}$, $\dot{\psi}$ measurements. For the position measurement, a PX4FLOW smart camera is added, which can provide the horizontal velocities $\dot{x}$, $\dot{y}$ and altitude z measurement. The sensor data reading and communication with the flight controller are done by an Arduino Due board. Since the PX4FLOW only provides the velocity measurements $\dot{x}$, $\dot{y}$, the position information x, y are estimated by integrating the velocity data. The vertical velocity $\dot{z}$ is estimated through differentiating the ultrasonic sensor measurement z.

5.1.2 Experimental Environment. The optical flow-based position estimation methods determine the motion of a quadrotor through calculating the visual flow from the sequences of ordered images taken from the camera. Thus, it is known that there are some limitations about the working conditions of the PX4FLOW sensor. It usually requires surfaces, where the images are taken, with clear patterns and adequate lighting to have good estimation results. Thus, the experimental environment, which is shown in Fig. 4, is built. The ground is covered by shelf liners to provide patterned images for the PX4FLOW sensor. Furthermore, four additional incandescent lamps are installed to provide enough lighting.

5.2 Filter Design and Controller Parameter Selection

5.2.1 Filter Design. According to Ref. [35], the choices of first-order low-pass filters in the form of

$$\begin{aligned} G_{\eta i}^f(s) &= \frac{1}{T_{\eta i}s + 1} \\ G_{\xi j}^f(s) &= \frac{1}{T_{\xi j}s + 1} \end{aligned} \tag{45}$$

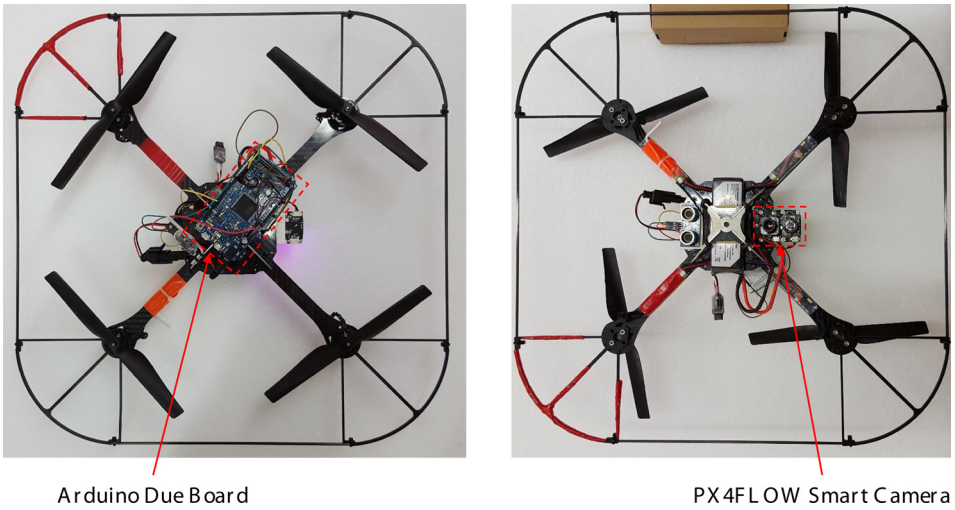

Fig. 3 Experimental platform: top view (left) and bottom view (right)

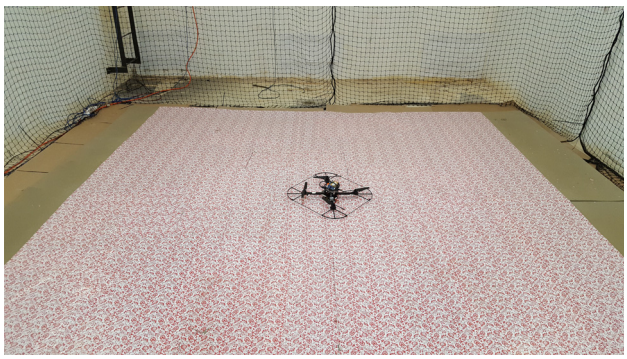

Fig. 4 Experimental environment with patterned surface on the ground

are reasonable, where $T_{\eta i}$ and $T_{\xi j}$ are the positive time constants that could be tuned to adjust the bandwidths of the low-pass filters. Then, the attitude controllers (21) are simplified as

$$u_{\eta i} = \frac{1}{B_{\eta i}}\left\{\left[\lambda_{\eta i}k_{\eta i} + \frac{\lambda_{\eta i}+k_{\eta i}}{T_{\eta i}}\right]e_{\eta i} + \frac{\lambda_{\eta i}k_{\eta i}}{T_{\eta i}}\int_0^t e_{\eta i}dt + \left(\lambda_{\eta i} + k_{\eta i} + \frac{1}{T_{\eta i}}\right)\dot{e}_{\eta i} + \ddot{\eta}_{ri}\right\} \tag{46}$$

where $i = 1\ldots3$ represent the ϕ, θ, and ψ, respectively. In order to facilitate implementation, $c_{\eta i}$ are introduced as positive constant coefficients that relate the speed difference commands in program to the generated torques. Thus, another design parameters are defined as $b_{\eta i} = c_{\eta i}/B_{\eta i}$.

The position controllers (28) are simplified as

$$u_{\xi j} = \frac{1}{B_{\xi j}}\bar{g}_j - \frac{1}{B_{\xi j}}\left\{\left[\lambda_{\xi j}k_{\xi j} + \frac{\lambda_{\xi j}+k_{\xi j}}{T_{\xi j}}\right]e_{\xi j} + \frac{\lambda_{\xi j}k_{\xi j}}{T_{\xi j}}\int_0^t e_{\xi j}dt + \left(\lambda_{\xi j} + k_{\xi j} + \frac{1}{T_{\xi j}}\right)\dot{e}_{\xi j} + \ddot{\xi}_{rj}\right\} \tag{47}$$

where $j = 1\ldots3$ represent the x, y, and z, respectively. Since $(1/B_{\xi 3})\bar{g}_3 = mg$, mg is compensated by a constant thrust command in implementation. $c_{\xi 3}$ is introduced as a positive constant coefficient that relates the thrust command in program to the generated thrust force. Thus, the design parameter for altitude control is defined as $b_{\xi 3} = c_{\xi 3}/B_{\xi 3}$. The roll and pitch reference angles for the attitude subsystems could be solved using Eqs. (22) and (23) as

$$\theta_r = \frac{u_x}{K_x\cos(\phi)}, \quad \phi_r = -\frac{1}{K_y}u_y \tag{48}$$

and $1/B_{\xi 1} = 1/B_{\xi 2} = m/F = (mg/F)(1/g)$. The ratio of mg/F could be easily calculated. Then, the design parameters $b_{\xi 1}$ and $b_{\xi 2}$ are introduced as $b_{\xi 1} = 1/K_x g$ and $b_{\xi 2} = 1/K_y g$. Let $T_1 = T_{\eta 1}, T_2 = T_{\eta 2}, T_3 = T_{\eta 3}, T_4 = T_{\xi 1}, T_5 = T_{\xi 2}, T_6 = T_{\xi 3}$ and $b_1 = b_{\eta 1}, b_2 = b_{\eta 2}, b_3 = b_{\eta 3}, b_4 = b_{\xi 1}, b_5 = b_{\xi 2}, b_6 = b_{\xi 3}$. Hence, there are six controllers (including four actual controllers F, τ_ϕ, τ_θ, τ_ψ, and two virtual controllers u_x, u_y) for the whole system with four parameters T_i, λ_i, k_i, and b_i that need tuning for each controller.

5.2.2 Controller Parameter Selection. From the control structures of the quadrotor system, which is shown in Fig. 2, it could be seen that the output of the horizontal position controllers are the roll, pitch angle references. It also implies that the good tracking performances of attitude controllers are very important for achieving the good position control performance. Thus, the three attitude controllers (46) are first tuned then followed by three position controllers (47). Since the six controllers are all UDE-based controllers, the parameter selection guidelines are similar. The choices of parameters are listed in Table 2, and the detailed parameter tuning procedures are described as follows:

(1) From the definition, it could be seen that b_i are related to the system parameters, such as inertia and mass. Since it is hard to get an accurate value b_i due to parameter uncertainties, the parameter selection starts with b_i being set to the nominal value of the system and an initial guess of the parameters λ_i, k_i, and T_i.

Table 2 UDE controller parameters

Dof	λ	T	k	b
ϕ	1	0.0160	10	0.0067
θ	1	0.0160	10	0.0067
ψ	1	0.0200	10	0.0200
z	1	0.0450	1	0.0010
x	1	0.0130	1	0.1000
y	1	0.0130	1	0.1000

Note: Dof: degrees-of-freedom.

(2) Since the first-order low-pass filters (45) are utilized to estimate the lumped uncertainty terms, in order to have good estimation results of the lumped uncertainty terms, the time constants of the filters T_i should be adjusted as small as possible such that the bandwidths of the filters are wide enough to cover the spectrum of the lumped uncertainty terms. However, in practice, reducing T_i will amplify the high frequency noises. Hence, the choice of the time constant T_i has a trade-off between the disturbance rejection performance and noise attenuation.

(3) From Eqs. (15), (12), and (27), it could be seen that the parameters k_i and λ_i specify the filtered tracking error convergence rates and the tracking error convergence rates. Thus, larger k_i and λ_i will result in faster system response and improve the tracking performance.

5.3 Results and Discussion

5.3.1 Case I: Attitude Stabilization. The control objective of this experiment is to stabilize the quadrotor attitude. Since the quadrotor controls its position through controlling the attitude angles, good attitude control performance is very important. The references for pitch, roll and yaw angles are set as $\theta_r = 0$ deg, $\phi_r = 0$ deg, and $\psi_r = 0$ deg. The first row of Fig. 5 shows the attitude variations and the second row shows the control inputs. The absolute values of the maximum tracking errors (AVMEs) and the root-mean-square errors (RMSEs) are listed in Table 3. The comparisons of RMSEs with the "First Flight Test: Hovering" case in Ref. [44] are shown in Table 4. Note that the hovering case in Ref. [44] was carried out with the roll, pitch references set to zero, which is similar to this case.

5.3.2 Case II: Hover. The control objective of this experiment is to make the quadrotor hover at the desired fixed point. The length of the experiment is about 60 s. The horizontal position references x_r and y_r are set to 0 m; the altitude reference z_r is set to -0.7 m, which is above the ground since the z positive axis is pointing toward the ground; and the heading angle reference ψ_r is set to 0 deg. Figure 6 shows the experimental results of the hover test. The first row represents the desired and actual position of the quadrotor. The position RMSEs are 0.030 m for x direction, 0.038 m for y direction, and 0.017 m for z direction and the AVMEs are 0.105 m for x direction, 0.109 m for y direction, and 0.045 m for z direction, which are also listed in Table 3. These are quite small tracking errors considering only onboard sensors are used. Since the PX4FLOW smart camera can only measure the x, y velocity information, the velocities of the quadrotor are shown in the second row of Fig. 6. The third row of Fig. 6 shows the desired and actual attitude angles. The calculated attitude RMSEs are shown in Table 3. The control inputs are plotted in Fig. 7. Figure 8 shows the horizontal coordinate plot for the hover test. It could be clearly seen that the quadrotor is able to maintain its horizontal position within a circle with the radius of 0.1 m. The experimental results have demonstrated the good performance of the UDE-based controllers for handling the model uncertainties and coupling effects. The comparisons of RMSEs with the "First Flight Test: Hovering" case in Ref. [44] are shown in Table 4. Note that in Ref. [44], the hovering experiments were carried out with roll, pitch references set to zero. While in this paper, since

Table 4 Comparisons of RMSEs with Ref. [44]

Dof	Case I	Case II	Hover [44]
ϕ	0.197 deg	0.355 deg	0.300 deg
θ	0.145 deg	0.266 deg	0.470 deg
ψ	0.088 deg	0.144 deg	—

Note: Dof: degrees-of-freedom.

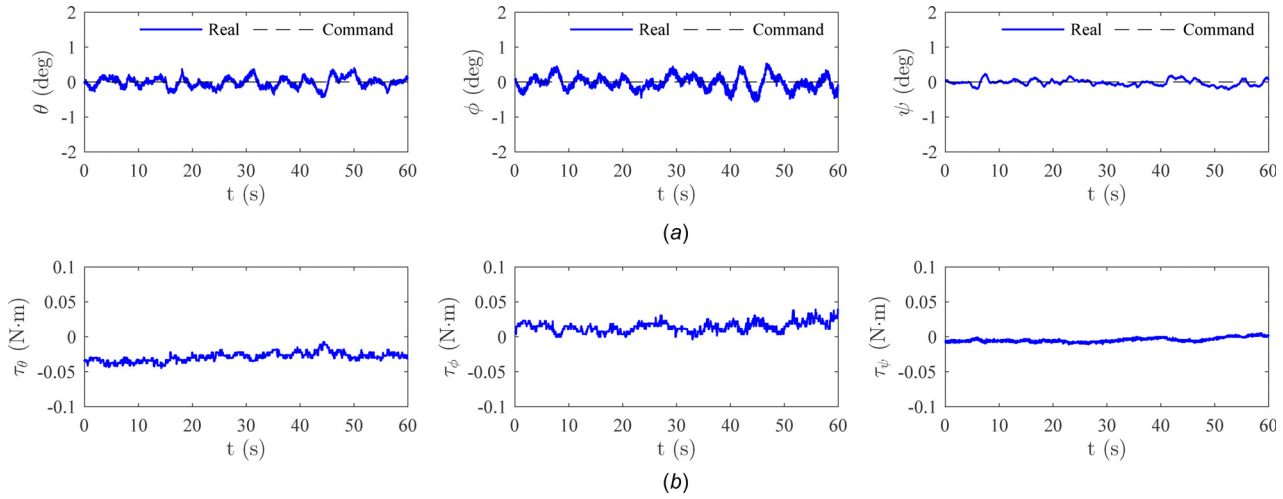

Fig. 5 Attitude stabilization: (*a*) attitude and (*b*) control input

Table 3 RMSEs and AVMEs of the experimental results

	Case I		Case II		Case III (a)	Case III (b)	Case IV	
Dof	RMSE	AVME	RMSE	AVME	RMSE	RMSE	RMSE	AVME
ϕ	0.197 deg	0.560 deg	0.355 deg	—	0.480 deg (35–40 s)	0.489 deg (35–40 s)	0.329 deg	—
θ	0.145 deg	0.430 deg	0.266 deg	—	0.394 deg (20–25 s)	0.504 deg (20–25 s)	0.274 deg	—
ψ	0.088 deg	0.235 deg	0.144 deg	—	0.239 deg (60–80 s)	0.148 deg (60–80 s)	0.168 deg	—
x	—	—	0.030 m	0.105 m	0.044 m (20–25 s)	0.037 m (20–25 s)	0.033 m	0.119 m
y	—	—	0.038 m	0.109 m	0.046 m (35–40 s)	0.044 m (35–40 s)	0.036 m	0.116 m
z	—	—	0.017 m	0.045 m	0.024 m (60–80 s)	0.022 m (60–80 s)	0.020 m	0.067 m

Note: Dof: degrees-of-freedom; RMSE: root-mean-square error; and AVME: absolute values of the maximum tracking error.

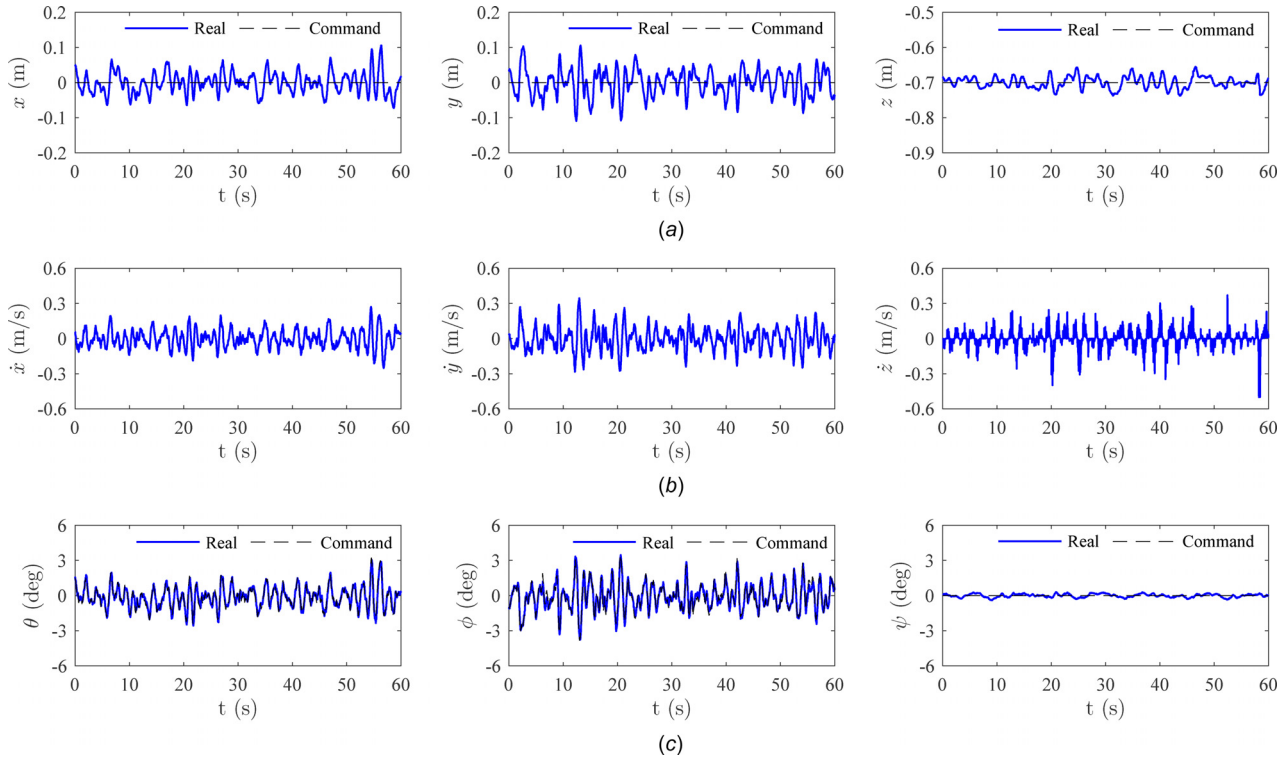

Fig. 6 Hover: (*a*) position, (*b*) velocity, and (*c*) attitude

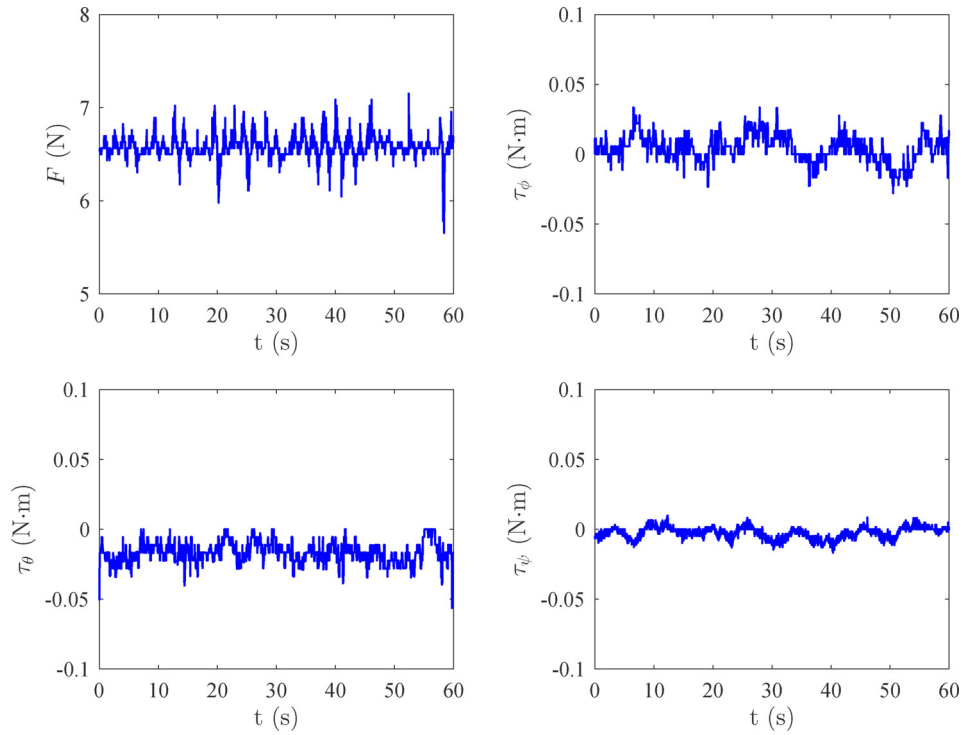

Fig. 7 Control inputs for the hover test

the full degrees-of-freedom of the quadrotor are considered. The roll and pitch controllers are required to constantly track the reference signals generated by the position controllers, which is more challenging.

5.3.3 Case III: Disturbance Rejection. To verify the disturbance rejection ability of the proposed controllers, two disturbance rejection cases are carried out with the input disturbances added to x, y controllers and roll, pitch attitude controllers, respectively. The experimental setup and controller parameters are the same with case II. The control objective of this experiment is to make the quadrotor hover at the desired fixed point under the effects of external disturbances. The length of the experiment is about 80 s. The horizontal position references x_r and y_r are set to 0 m; the altitude reference z_r is set to -0.7 m; and the heading angle reference ψ_r is set to 0 deg.

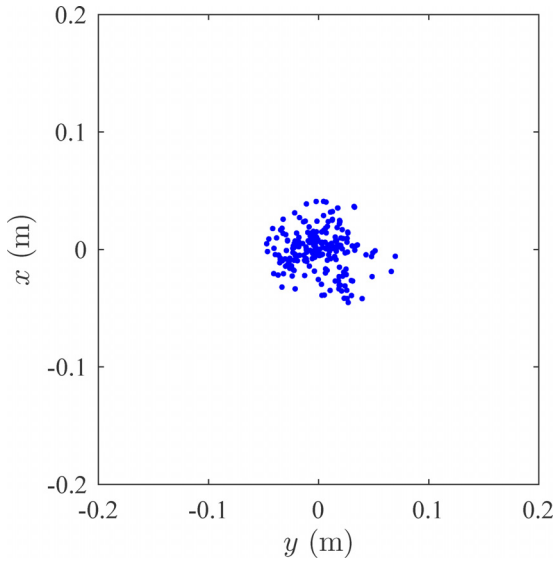

Fig. 8 Horizontal coordinate plot for the hover test

(a) Input disturbance applied on the position controller. The experimental results are shown in Fig. 9. There are no disturbances applied in the first 10 s. The step input disturbance with the magnitude of 8 deg is applied to x controller at 10 s and disabled at 40 s and applied to y controller at 25 s and disabled at 55 s. The first and second rows of Fig. 9 show the positions and velocities of the quadrotor during disturbance rejection: position controller test. The peak values after the disturbances applied and disabled are -0.566 m (10 s) and 0.634 m (40 s) for x direction and 0.670 m (25 s) and -0.634 m (55 s) for y direction. The quadrotor is able to maintain stable after the disturbances applied and recover to the desired positions within 5 s. The third row of Fig. 9 shows the attitude variations and commands. Since the commands of the pitch and roll angles are generated by the x, y position controllers and disturbances are added as input disturbances, it could be clearly seen from the pitch and roll commands that the added input disturbances are successfully compensated by the developed UDE-based position controllers. The calculated steady-state position and attitude RMSEs after the disturbances applied are shown in Table 3. Figure 10 shows the control inputs.

(b) Input disturbance applied on the attitude controller. Due to the coupling between position and attitude of the quadrotor, the disturbances added to the roll, pitch attitude controllers will also affect the x, y positions of the quadrotor. The experimental results are shown in Fig. 11. There are no disturbances applied in the first 10 s. The step input disturbances with the magnitude of 40% of the maximum pitch (roll), which are equivalent to 0.225 N·m, are applied to pitch controller at 10 s and disabled at 40 s and applied to roll controller at 25 s and disabled at 55 s. The first and second rows of Fig. 11 show the positions and velocities of the quadrotor during disturbance rejection: attitude controller test. The peak values after the disturbances applied and disabled are 0.442 m (10 s) and -0.480 m (40 s) for x direction and 0.518 m (25 s) and -0.547 m (55 s) for y direction. The quadrotor is able to maintain stable after the disturbances applied and recover to the desired positions within 5 s. The third row of Fig. 11 shows the attitude variations and its references. The steady-state position and attitude RMSEs are calculated in Table 3. Figure 12 shows the control inputs. From Fig. 12, it could be seen that the added input disturbances are successfully compensated by the developed UDE-based attitude controllers. The experimental results of two disturbance rejection cases have demonstrated the good robust performance of the UDE-based controllers for handling large disturbance and formidable reliability of the developed control system.

5.3.4 Case IV: Trajectory Tracking. To verify the tracking performance of the developed UDE-based controller, the trajectory tracking experiment is performed. The desired trajectory is a

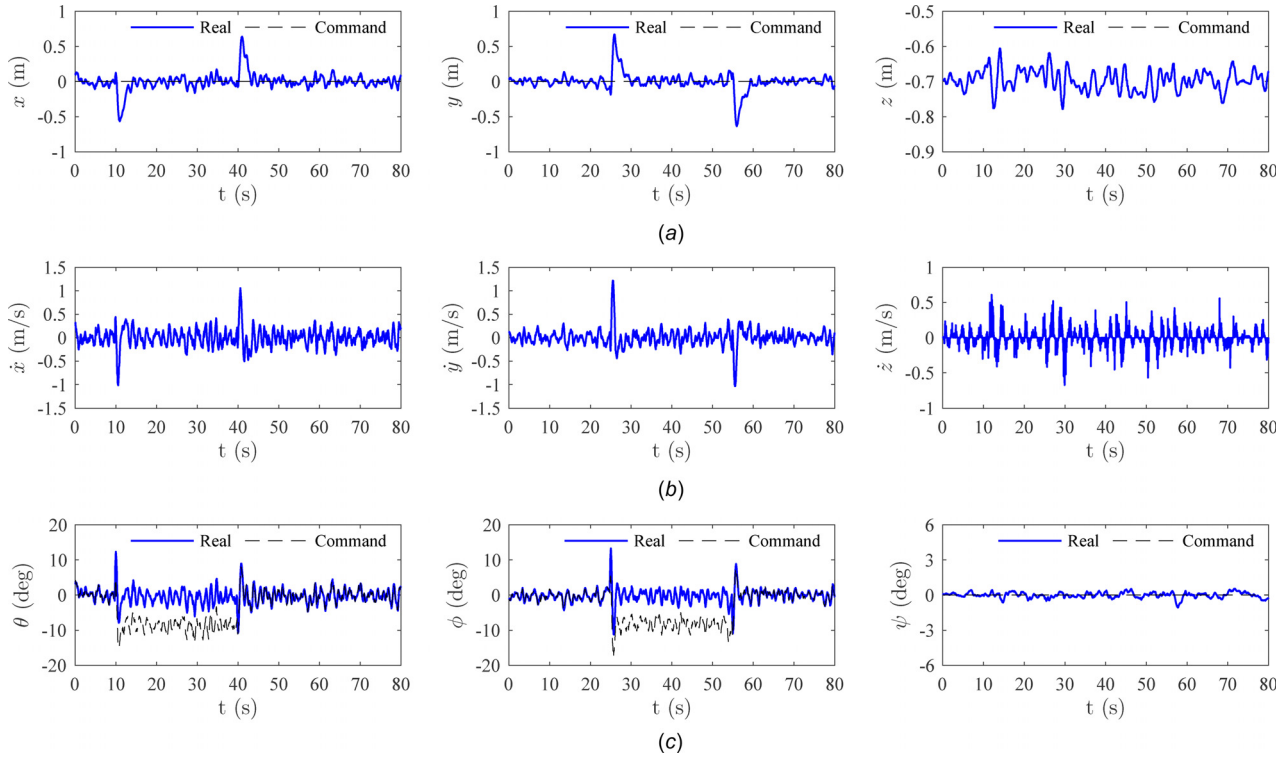

Fig. 9 Disturbance rejection: position controller (*a*) position, (*b*) velocity, and (*c*) attitude

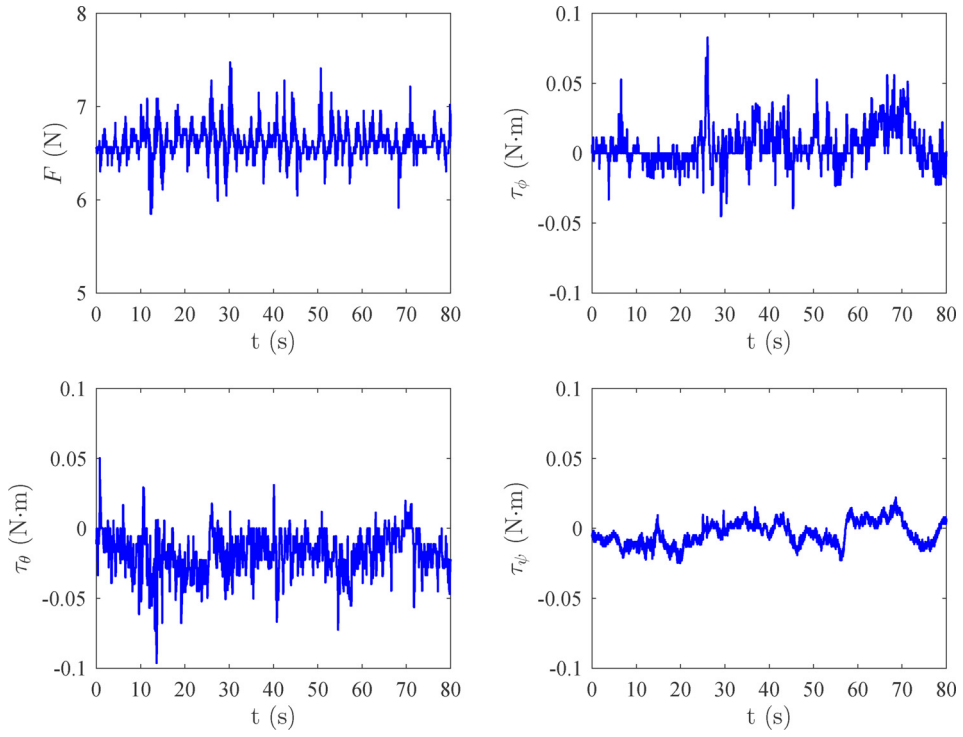

Fig. 10 Control inputs for the disturbance rejection: position controller test

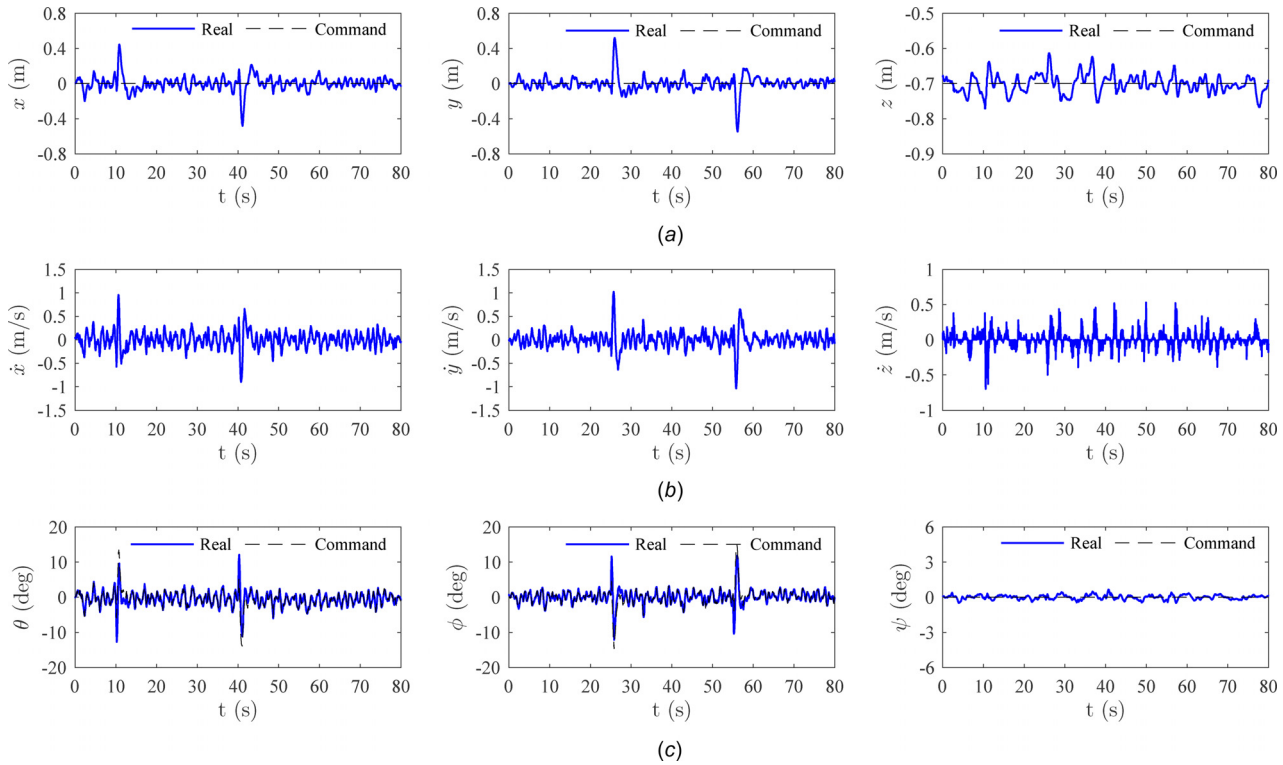

Fig. 11 Disturbance rejection: attitude controller (*a*) position, (*b*) velocity, and (*c*) attitude

circle with the diameter of 1.6 m. There are no disturbances applied. The control objective of this experiment is to make the quadrotor follow the desired trajectory. The experimental setup and controller parameters are the same with case II. The altitude reference z_r is set to -0.7 m and the heading angle reference ψ_r is set to 0 deg. The experimental results are shown in Fig. 13. The first, second, and third row of Fig. 13 show, respectively, the positions, velocities, and desired/actual attitude angles of the quadrotor for trajectory tracking test. The calculated position RMSEs, position AVMEs, and attitude RMSEs are shown in Table 3. The control inputs of the trajectory tracking case are shown in Fig. 14. Figure 15 shows the horizontal coordinate of the quadrotor for the trajectory tracking test. It could be seen that the developed UDE-based controllers could successfully track the

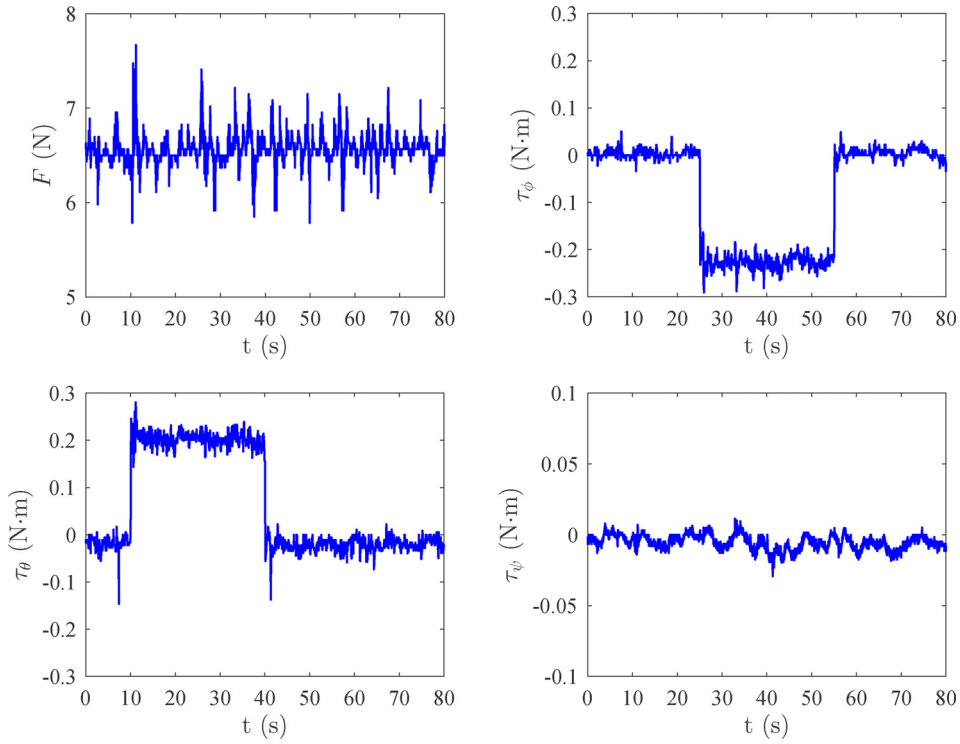

Fig. 12 Control inputs for the disturbance rejection: attitude controller test

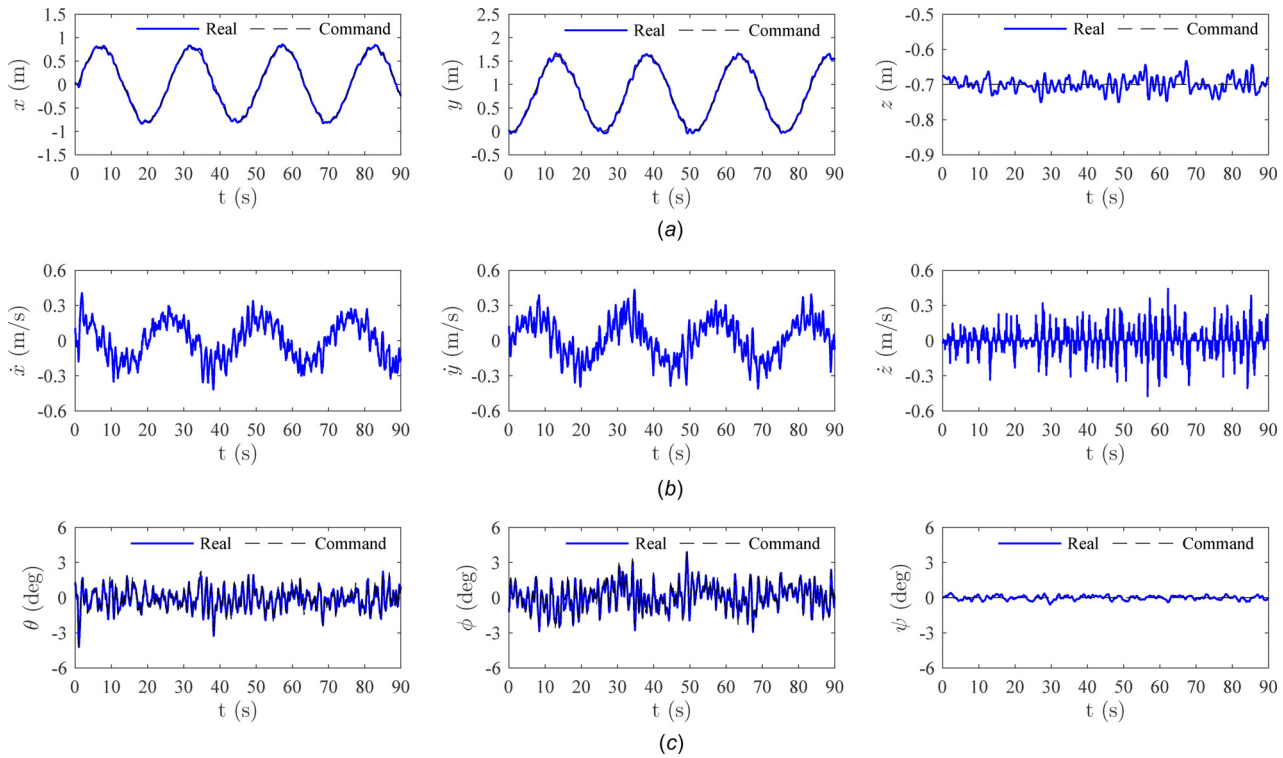

Fig. 13 Trajectory tracking (*a*) position, (*b*) velocity, and (*c*) attitude

desired trajectory while maintaining the desired altitude and heading angle.

5.3.5 Case V: Comparison With the Proportional–Integral–Derivative Controller. In order to further demonstrate the flexibility and advantages of the UDE-based controllers, the comparative experiments with PID controller are carried out. The control objective of this case is to make the quadrotor hover at the desired fixed point under the effects of sinusoidal disturbances. The horizontal position references x_r and y_r are set to 0 m and the altitude reference z_r is set to -0.7 m. The PID controllers in the form of $u_{\xi j}^{\mathrm{PID}} = k_{\xi j}^{\mathrm{P}} e_{\xi j} + k_{\xi j}^{\mathrm{I}} \int_0^t e_{\xi j} dt - k_{\xi j}^{\mathrm{D}} \dot{\xi}_j$ are implemented for the position

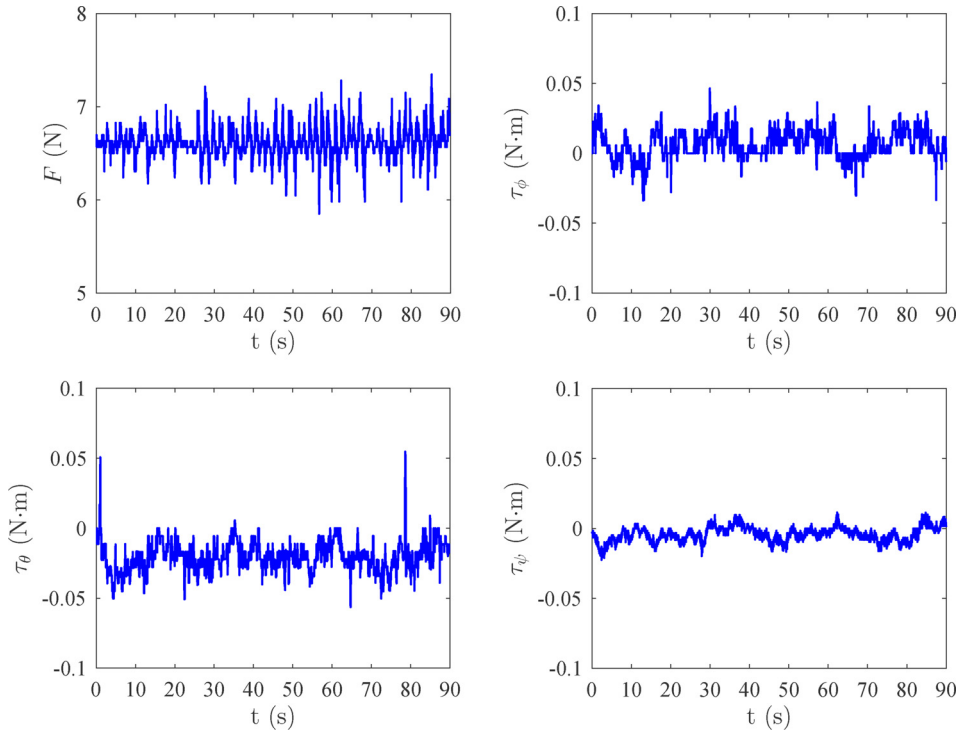

Fig. 14 Control inputs for the trajectory tracking test

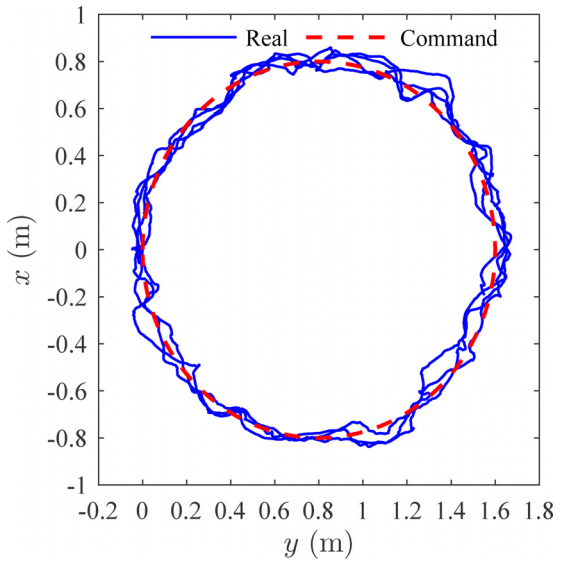

Fig. 15 Horizontal coordinate plot for the trajectory tracking test

control of the quadrotor, where $j = 1 \ldots 3$ represent the x, y, and z, respectively. The PID controller parameters are listed in Table 5. In order to handle the sinusoidal disturbance, the filters for the UDE-based controllers are redesigned according to the well-known internal model principle [45,46] as

$$G^f_{\xi j}(s) = 1 - \left(\frac{s}{s + \frac{1}{T_{\xi j}}}\right)\left(\frac{s^2 + \omega^2_{\xi j}}{s^2 + \frac{\omega_{\xi j}}{Q_{\xi j}} s + \omega^2_{\xi j}}\right) \tag{49}$$

which are implemented on the horizontal position x and y controllers. The parameters for the UDE-based controllers are set as $k_{\xi 1} = k_{\xi 2} = 0.09$, $\lambda_{\xi 1} = \lambda_{\xi 2} = 0.7$, $T_{\xi 1} = T_{\xi 2} = 0.0118$, $\omega_{\xi 1} = \omega_{\xi 2} = 0.2\pi$, and $Q_{\xi 1} = Q_{\xi 2} = 1$ to have similar performance with the PID controllers in the nominal case, where no disturbance is applied, for fair comparison. Then, the disturbance rejection experiments are carried out with the input sinusoidal disturbances added to the x and y controllers without changing the controller parameters. The magnitude and frequency of the input disturbances are 5 deg and 0.1 Hz, respectively. The experimental results are shown in Fig. 16. The CMD is short for Command, which specifies the desired positions. The thin and thick solid lines show the experimental results of the UDE-based controller and the PID controller, respectively. The controller for the z direction is PID controller for all experimental cases. Since the comparisons are only carried out on x and y directions, to make the presentation of the experimental results more clear, the altitude of the quadrotor is not shown. The first row of Fig. 16 shows the nominal case, where there is no disturbance applied. It should be noted that in the nominal case, the PID controller and the UDE-based controller have similar performance. From the second row of Fig. 16, which shows the disturbance rejection experimental results, it could be seen that the UDE-based controller could successfully handle the sinusoidal disturbances while the PID controller exhibits large periodic errors. The experimental results have demonstrated the robustness and superiority of the UDE-based controller over the PID controller for handling sinusoidal disturbances.

Table 5 PID controller parameters

Dof	k^{P}_{ξ}	k^{I}_{ξ}	k^{D}_{ξ}
x	6.7213	0.5355	8.5790
y	6.7213	0.5355	8.5790
z	0.0180	0.0200	0.0028

Note: Dof: degrees-of-freedom.

6 Conclusions

In this paper, the UDE-based cascaded robust control scheme was developed and applied for the quadrotor trajectory tacking

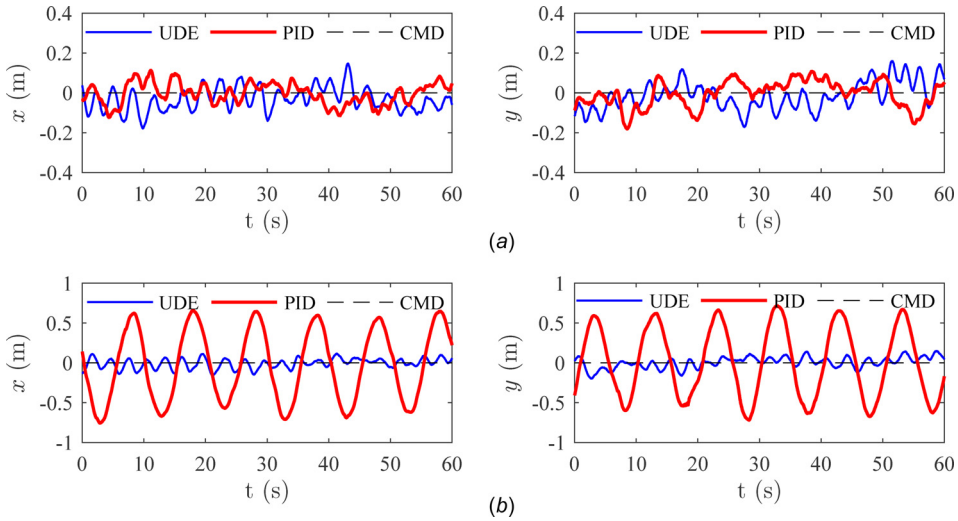

Fig. 16 Comparison with the PID controller for the hover test (*a*) nominal case and (*b*) sinusoidal disturbance rejection

control in a GPS-denied environment using solely onboard sensing. First, a high-speed optical flow sensor PX4FLOW was adopted to achieve the accurate estimation of the quadrotor positions. Then the UDE-based controllers were developed to deal with the problems of coupled dynamics, internal uncertainties, nonaffine inputs and external disturbances. Furthermore, the filtered tracking error dynamics has been introduced to simplify the controller design and implementation. The effectiveness of the developed controller has been verified through extensive experimental studies with five cases considered, attitude stabilization, hover, disturbance rejection, trajectory tracking and comparison with the PID controller. The experimental results demonstrated the remarkable capabilities of developed controllers for handling the aforementioned challenges simultaneously and satisfactorily.

Acknowledgment

The authors would like to sincerely thank the Editors and the Reviewers for their insightful and constructive comments, which have helped to greatly improve the quality of the paper.

References

[1] Erginer, B., and Altug, E., 2007, "Modeling and PD Control of a Quadrotor VTOL Vehicle," IEEE Intelligent Vehicles Symposium (IVS), Istanbul, Turkey, June 13–15, pp. 894–899.
[2] Bouabdallah, S., 2007, "Design and Control of Quadrotors With Application to Autonomous Flying," Ph.D. thesis, École Polytechnique Federale de Lausanne, Lausanne, Switzerland.
[3] Blösch, M., Weiss, S., Scaramuzza, D., and Siegwart, R., 2010, "Vision Based MAV Navigation in Unknown and Unstructured Environments," IEEE International Conference on Robotics and Automation (ICRA), Anchorage, AK, May 3–7, pp. 21–28.
[4] Hoffmann, G. M., Huang, H., Waslander, S. L., and Tomlin, C. J., 2007, "Quadrotor Helicopter Flight Dynamics and Control: Theory and Experiment," AIAA Paper No. 2007-6461.
[5] Hoffmann, G. M., Huang, H., Waslander, S. L., and Tomlin, C. J., 2011, "Precision Flight Control for a Multi-Vehicle Quadrotor Helicopter Testbed," Control Eng. Practice, **19**(9), pp. 1023–1036.
[6] Mebarki, R., Lippiello, V., and Siciliano, B., 2015, "Nonlinear Visual Control of Unmanned Aerial Vehicles in GPS-Denied Environments," IEEE Trans. Rob., **31**(4), pp. 1004–1017.
[7] Honegger, D., Meier, L., Tanskanen, P., and Pollefeys, M., 2013, "An Open Source and Open Hardware Embedded Metric Optical Flow CMOS Camera for Indoor and Outdoor Applications," IEEE International Conference on Robotics and Automation (ICRA), Karlsruhe, Germany, May 6–10, pp. 1736–1741.
[8] Choi, Y.-C., and Ahn, H.-S., 2015, "Nonlinear Control of Quadrotor for Point Tracking: Actual Implementation and Experimental Tests," IEEE/ASME Trans. Mechatronics, **20**(3), pp. 1179–1192.
[9] Yun, B., Peng, K., and Chen, B. M., 2007, "Enhancement of GPS Signals for Automatic Control of a UAV Helicopter System," IEEE International Conference on Control and Automation (ICCA), Guangzhou, China, May 30–June 1, pp. 1185–1189.
[10] Michael, N., Mellinger, D., Lindsey, Q., and Kumar, V., 2010, "The GRASP Multiple Micro-UAV Testbed," IEEE Rob. Autom. Mag., **17**(3), pp. 56–65.
[11] Goodarzi, F. A., Lee, D., and Lee, T., 2015, "Geometric Adaptive Tracking Control of a Quadrotor UAV on SE (3) for Agile Maneuvers," ASME J. Dyn. Syst. Meas. Control, **137**(9), p. 091007.
[12] Islam, S., Liu, P., and El Saddik, A., 2015, "Robust Control of Four-Rotor Unmanned Aerial Vehicle With Disturbance Uncertainty," IEEE Trans. Ind. Electron., **62**(3), pp. 1563–1571.
[13] Ozaslan, T., Shen, S., Mulgaonkar, Y., Michael, N., and Kumar, V., 2015, "Inspection of Penstocks and Featureless Tunnel-Like Environments Using Micro UAVs," Conference on Field and Service Robotics, Brisbane, Australia, Dec. 9–11, pp. 123–136.
[14] Shen, S., Michael, N., and Kumar, V., 2011, "Autonomous Multi-Floor Indoor Navigation With a Computationally Constrained MAV," IEEE International Conference on Robotics and Automation (ICRA), Shanghai, China, May 9–13, pp. 20–25.
[15] Dryanovski, I., Morris, W., and Xiao, J., 2011, "An Open-Source Pose Estimation System for Micro-Air Vehicles," IEEE International Conference on Robotics and Automation (ICRA), Shanghai, China, May 9–13, pp. 4449–4454.
[16] Bachrach, A., He, R., and Roy, N., 2009, "Autonomous Flight in Unknown Indoor Environments," Int. J. Micro Air Veh., **1**(4), pp. 217–228.
[17] Ozaslan, T., Loianno, G., Keller, J., Taylor, C. J., Kumar, V., Wozencraft, J. M., and Hood, T., 2017, "Autonomous Navigation and Mapping for Inspection of Penstocks and Tunnels With MAVs," IEEE Rob. Autom. Lett., **2**(3), pp. 1740–1747.
[18] Zhang, X., Xian, B., Zhao, B., and Zhang, Y., 2015, "Autonomous Flight Control of a Nano Quadrotor Helicopter in a GPS-Denied Environment Using On-Board Vision," IEEE Trans. Ind. Electron., **62**(10), pp. 6392–6403.
[19] Floreano, D., Zufferey, J.-C., Srinivasan, M. V., and Ellington, C., 2009, *Flying Insects and Robots*, Springer-Verlag, Berlin.
[20] Xian, B., Liu, Y., Zhang, X., Cao, M., and Wang, F., 2014, "Hovering Control of a Nano Quadrotor Unmanned Aerial Vehicle Using Optical Flow," Chinese Control Conference (CCC), Nanjing, China, July 28–30, pp. 8259–8264.
[21] Kendoul, F., Fantoni, I., and Nonami, K., 2009, "Optic Flow-Based Vision System for Autonomous 3D Localization and Control of Small Aerial Vehicles," Rob. Auton. Syst., **57**(6), pp. 591–602.
[22] Garrido-Jurado, S., Munoz-Salinas, R., Madrid-Cuevas, F. J., and Marin-Jimenez, M. J., 2014, "Automatic Generation and Detection of Highly Reliable Fiducial Markers Under Occlusion," Pattern Recognit., **47**(6), pp. 2280–2292.
[23] Ascending Technologies, 2015, "AscTec Hummingbird," Ascending Technologies GmbH, Krailling, Germany, accessed Sept. 1, 2017, http://www.asctec.de/en/
[24] Bouabdallah, S., Noth, A., and Siegwart, R., 2004, "PID vs LQ Control Techniques Applied to an Indoor Micro Quadrotor," IEEE/RSJ International Conference on Intelligent Robots and Systems (IROS), Sendai, Japan, Sept. 28–Oct. 2, pp. 2451–2456.
[25] Castillo, P., Dzul, A., and Lozano, R., 2004, "Real-Time Stabilization and Tracking of a Four-Rotor Mini Rotorcraft," IEEE Trans. Control Syst. Technol., **12**(4), pp. 510–516.
[26] Zhao, B., Xian, B., Zhang, Y., and Zhang, X., 2015, "Nonlinear Robust Adaptive Tracking Control of a Quadrotor UAV Via Immersion and Invariance Methodology," IEEE Trans. Ind. Electron., **62**(5), pp. 2891–2902.
[27] Das, A., Subbarao, K., and Lewis, F., 2009, "Dynamic Inversion With Zero-Dynamics Stabilisation for Quadrotor Control," IET Control Theory Appl., **3**(3), pp. 303–314.
[28] Bouabdallah, S., and Siegwart, R., 2007, "Full Control of a Quadrotor," IEEE/RSJ International Conference on Intelligent Robots and Systems (IROS), San Diego, CA, Oct. 29–Nov. 2, pp. 153–158.
[29] Ramirez-Rodriguez, H., Parra-Vega, V., Sanchez-Orta, A., and Garcia-Salazar, O., 2014, "Robust Backstepping Control Based on Integral Sliding Modes for Tracking of Quadrotors," J. Intell. Rob. Syst., **73**(1), pp. 51–66.

[30] Dydek, Z. T., Annaswamy, A. M., and Lavretsky, E., 2013, "Adaptive Control of Quadrotor UAVs: A Design Trade Study With Flight Evaluations," IEEE Trans. Control Syst. Technol., **21**(4), pp. 1400–1406.
[31] Besnard, L., Shtessel, Y. B., and Landrum, B., 2012, "Quadrotor Vehicle Control Via Sliding Mode Controller Driven by Sliding Mode Disturbance Observer," J. Franklin Inst., **349**(2), pp. 658–684.
[32] Liu, H., Wang, X., and Zhong, Y., 2015, "Quaternion-Based Robust Attitude Control for Uncertain Robotic Quadrotors," IEEE Trans. Ind. Inf., **11**(2), pp. 406–415.
[33] Lee, K., Back, J., and Choy, I., 2014, "Nonlinear Disturbance Observer Based Robust Attitude Tracking Controller for Quadrotor UAVs," Int. J. Control, Autom. Syst., **12**(6), pp. 1266–1275.
[34] Dong, W., Gu, G.-Y., Zhu, X., and Ding, H., 2014, "High-Performance Trajectory Tracking Control of a Quadrotor With Disturbance Observer," Sens. Actuators A, **211**, pp. 67–77.
[35] Zhong, Q.-C., and Rees, D., 2004, "Control of Uncertain LTI Systems Based on an Uncertainty and Disturbance Estimator," ASME J. Dyn. Syst. Meas. Control, **126**(4), pp. 905–910.
[36] Stobart, R., Kuperman, A., and Zhong, Q.-C., 2011, "Uncertainty and Disturbance Estimator–Based Control for Uncertain LTI-SISO Systems With State Delays," ASME J. Dyn. Syst. Meas. Control, **133**(2), p. 024502.
[37] Talole, S., Chandar, T. S., and Kolhe, J. P., 2011, "Design and Experimental Validation of UDE Based Controller-Observer Structure for Robust Input-Ouput Linearisation," Int. J. Control, **84**(5), pp. 969–984.
[38] Talole, S., and Phadke, S., 2009, "Robust Input-Output Linearisation Using Uncertainty and Disturbance Estimation," Int. J. Control, **82**(10), pp. 1794–1803.
[39] Ren, B., Zhong, Q.-C., and Chen, J., 2015, "Robust Control for a Class of Non-Affine Nonlinear Systems Based on the Uncertainty and Disturbance Estimator," IEEE Trans. Ind. Electron., **62**(9), pp. 5881–5888.
[40] Kuperman, A., and Zhong, Q.-C., 2011, "Robust Control of Uncertain Nonlinear Systems With State Delays Based on an Uncertainty and Disturbance Estimator," Int. J. Robust Nonlinear Control, **21**(1), pp. 79–92.
[41] Kolhe, J. P., Shaheed, M., Chandar, T. S., and Taloe, S. E., 2013, "Robust Control of Robot Manipulators Based on Uncertainty and Diturbance Estimation," Int. J. Robust Nonlinear Control, **23**(1), pp. 104–122.
[42] Lu, Q., Ren, B., Parameswaran, S., and Zhong, Q.-C., 2016, "Robust Position Control of a Quadrotor Using Onboard Optical Flow Sensor," ASME Paper No. DSCC2016-9812.
[43] Dai, J., Lu, Q., Ren, B., and Zhong, Q.-C., 2015, "Robust Attitude Tracking Control for a Quadrotor Based on the Uncertainty and Disturbance Estimator," ASME Paper No. DSCC2015-9900.
[44] Sanz, R., Garcia, P., Zhong, Q.-C., and Albertos, P., 2016, "Robust Control of Quadrotors Based on an Uncertainty and Disturbance Estimator," ASME J. Dyn. Syst. Meas. Control, **138**(7), p. 071006.
[45] Ren, B., Zhong, Q.-C., and Dai, J., 2017, "Asymptotic Reference Tracking and Disturbance Rejection of UDE-Based Robust Control," IEEE Trans. Ind. Electron., **64**(4), pp. 3166–3176.
[46] Francis, B. A., and Wonham, W. M., 1976, "The Internal Model Principle of Control Theory," Automatica, **12**(5), pp. 457–465.